Conf-9206161--1

COMPUTER MODEL SIMULATION OF NULL-FLUX MAGNETIC SUSPENSION AND GUIDANCE

J.L. He and D.M. Rote

Center for Transportation Research, Energy Systems Division
Argonne National Laboratory, Argonne, IL, 60439, USA

ANL/CP--73256

DE92 013044

to be presented at
the 6th World Conference on Transport Research
June 29 -July 3 1992

DISCLAIMER

COMPUTER MODEL SIMULATION OF NULL-FLUX MAGNETIC SUSPENSION AND GUIDANCE

Jianliang HE
Electrical Engineer

Donald M. ROTE
Physicist

Center for Transportation Research, Energy Systems Division
Argonne National Laboratory, Argonne, Illinois 60439, USA

ABSTRACT

This paper discusses the magnetic force computations in a null-flux suspension system using dynamic circuit theory. A computer simulation model that can be used to compute magnetic forces and predict the system performance is developed on the basis of dynamic circuit theory. Numerical examples are presented to demonstrate the application of the model. The performance of the null-flux suspension system is simulated and discussed.

1. INTRODUCTION

Null-flux coil arrangements are an important class of guideway conductor configuration for maglev designs incorporating electrodynamic suspension (EDS) systems. The concept of using flat and folded figure-eight shaped null-flux coils in conjunction with EDS systems was invented by Powell and Danby in the late 1960s [1]. A maglev design concept utilizing a separate set of horizontal null-flux loops for lateral guidance was put forward by the Canadian maglev design group in the late 1970s. Subsequently, they replaced the separate null-flux loops with cross-connected propulsion windings mounted vertically on the guideway to improve the guidance forces [2]. The MLU001 and MLU002 maglev vehicles built by the Japanese were tested at Miyazaki in the 1980s. The Muyazaki test track incorporated cross-connected propulsion windings for lateral guidance. In 1988 and 1989 they reported on analytical studies and the first test of the MLU002 vehicle utilizing side-wall mounted figure-eight null-flux coils for both suspension and lateral guidance [3-7]. A similar side-wall mounted null-flux system is planned for the new 41-km test track in the Yamanashi Prefecture. The major features of the null-flux suspension system are its simple configuration and its capacity to provide both suspension and guidance forces with a high lift-to-drag ratio. In particular, it can provide zero magnetic drag at the null-flux equilibrium point, hence, making the start-up of the maglev vehicle more efficient.

A maglev vehicle uses magnetic forces to perform three functions: propulsion, levitation, and guidance. Two commonly used approaches for the computation of magnetic forces are the electromagnetic field approach and the electrical circuit approach. The dynamic circuit model is a circuit approach in which the circuit components involve relative motion, and the circuit parameters are functions of displacement and time. The main advantage of the dynamic circuit model over other methods is that it can simulate the transient and dynamic performance of an electromagnetic or electromechanical system in a relatively simple manner The model is especially suited for the EDS maglev system involving coil-shaped components. In dynamic circuit theory, all of the flux links

between any two coils in the system are represented by the time-varying position-dependent mutual inductances of the two coils; for instance, the flux cancellation between the upper and the lower loop of the figure-eight null-flux coil is represented by two mutual inductances connected in opposite polarity. Furthermore, all magnetic forces in the system are considered to be generated as a result of the change of the magnetic energies stored in the system or the changes of mutual inductances between the coils.

The computations of magnetic forces using dynamic circuit theory for various suspension systems were discussed in a previous paper [8]. This paper addresses the computation of the figure-eight-shaped null-flux coil suspension system. First, the computer model for the null-flux suspension based on the dynamic circuit theory is described. Then numerical examples are presented to demonstrate the capability of the model and to predict the performance of the null-flux suspension system. Comments and future work are discussed in the conclusion section.

2. DYNAMIC CIRCUIT MODEL APPLICATION TO THE FIGURE-EIGHT NULL-FLUX COIL SUSPENSIONS

The two most commonly discussed null-flux suspension configurations are the flat figure-eight-shaped null-flux coil configuration and the folded figure-eight-shaped null-flux coil configuration; these are shown in Fig. 1 and Fig. 2, respectively. Both geometries follow the same operation principle, that is, the flux produced by the upper loop coil always opposes that produced by the lower loop coil. The null-flux magnetic lift forces are thus generated to return a moving superconducting magnet (SCM) to the equilibrium position when it is displaced from the balanced position. One can describe both flat and folded null-flux coil suspensions by the dynamic circuit model as shown in Fig. 3, in which one can assume, for general purposes, that m moving superconducting coils interact with n null-flux coils consisting of 2n loops. In this model, each superconducting coil is represented by a constant current source, mutual inductances exist between any two loops, and the polarity of each inductor is indicated by a dot at its end. It should be noted that Fig. 3 can describe the configuration in both Fig. 1 and Fig. 2, however, the dynamic circuit parameters in Fig.3 are different for the two configurations.

Considering a general case in which m SCMs aboard a vehicle interact with n short-circuited guideway coils to produce either levitation or guidance forces, one can write the system voltage equations in matrix form based on Kirchhoff's voltage law as:

$$[R][i] + [L]\frac{d}{dt}[i] + v_x[G_x][I] + v_y[G_y][I] + v_z[G_z][I] = 0 \qquad (1)$$

where [i] and [I] are column matrices composed of n unknown guideway coil currents and m specified superconducting coil currents, respectively; [L] is a square (nxn) matrix, each element of which represents either the self-inductances or mutual inductances of the guideway coils; [R] is a diagonal n-element matrix composed of the individual guideway coil resistances; v_x, v_y, and v_z are the velocities of the vehicle in the x, y, and z directions, respectively; and $[G_x]$, $[G_y]$ and $[G_z]$ are (nxm) matrices, each element of which represents the derivative of the mutual inductance between the guideway and the vehicle coils with respect to x, y, and z, respectively. General expressions for the three time-varying magnetic force components f_x, f_y, and f_y acting on the vehicle coils are [8]:

$$f_x = [i]^T[G_x][I] \qquad (2)$$

$$f_y = [\,i\,]^T[G_y][\,I\,] \tag{3}$$

$$f_z = [\,i\,]^T[G_z][\,I\,] \tag{4}$$

According to the conventional notation, we may refer to f_x as the force in the direction of motion, the average of which could be a magnetic drag force; f_y as the force in the horizontal direction, which could be a guidance or a lateral perturbation force; and f_z as the force in the vertical direction, representing a levitation or a vertical perturbation force.

The n figure-eight null-flux coils comprise 2n loops, and one can number the upper loop coils from 1 to n and the lower loop coils from n+1 to 2n. Applying Eq. (1) to Eq. (4) to the null-flux system as shown in Fig. 3 and neglecting the vertical and lateral speed v_z and v_y, respectively, one obtains for the voltage equations:

$$\begin{bmatrix} R & & \\ & R & \\ & \cdots & \\ & & R \end{bmatrix}\begin{bmatrix} i_1 \\ i_2 \\ \cdots \\ i_n \end{bmatrix} + \begin{bmatrix} L_{1,1}-L_{1,n+1} & L_{1,2}-L_{1,n+2} & \cdots & L_{1,n}-L_{1,2n} \\ L_{2,1}-L_{2,n+1} & L_{2,2}-L_{2,n+2} & & L_{2,n}-L_{2,2n} \\ \cdots & \cdots & \cdots & \cdots \\ L_{n,1}-L_{n,n+1} & \cdots & \cdots & L_{n,n}-L_{n,2n} \end{bmatrix}\frac{d}{dt}\begin{bmatrix} i_1 \\ i_2 \\ \cdots \\ i_n \end{bmatrix} =$$

$$-\frac{v_x}{2}\begin{bmatrix} G_{1,1}-G_{n+1,1} & G_{1,2}-G_{n+1,2} & \cdots & G_{1,m}-G_{n+1,m} \\ G_{2,1}-G_{n+2,1} & G_{2,2}-G_{n+2,2} & & G_{2,m}-G_{n+2,m} \\ \cdots & \cdots & \cdots & \cdots \\ G_{n,1}-G_{2n,1} & \cdots & \cdots & G_{n,m}-G_{2n,m} \end{bmatrix}\begin{bmatrix} I_1 \\ I_2 \\ \cdots \\ I_m \end{bmatrix} \tag{5}$$

For the time-varying magnetic forces one obtains:

$$f_x = \sum_{i=1}^{n}\sum_{j=1}^{m} i_i\, I_j\left[\frac{\partial L_{i,j}}{\partial x} - \frac{\partial L_{n+i,j}}{\partial x}\right] \tag{6}$$

$$f_y = \sum_{i=1}^{n}\sum_{j=1}^{m} i_i\, I_j\left[\frac{\partial L_{i,j}}{\partial y} - \frac{\partial L_{n+i,j}}{\partial y}\right] \tag{7}$$

$$f_z = \sum_{i=1}^{n}\sum_{j=1}^{m} i_i\, I_j\left[\frac{\partial L_{i,j}}{\partial z} - \frac{\partial L_{n+i,j}}{\partial z}\right] \tag{8}$$

where R is the resistance of a single loop coil, L_{ij} (i=1,n and j=1,n) are the self-inductances of the loops or the mutual inductances between the loops, and G_{ij} (i=1,n and j=1,m) are the derivatives of the mutual inductances between the loops and the moving superconducting coils.

Several important points should be noted from Eq. (5) to Eq. (8). First, the currents induced in the null-flux coils are due to the speed voltages in the right-hand side of Eq. (5). The speed voltages are given by the product of the vehicle speed v_x, the

superconducting coil current I_j (j=1,m), and the derivative of the mutual inductance between the moving vehicle coils and the stationary guideway coils. This means that the suspension forces depend upon the product of the above three factors. Secondly, the currents in the null-flux coils are reduced substantially when compared with the currents induced in a normal flux, single loop-shaped coil guideway because of the flux cancellation between the upper and lower loops. This is also seen from Eq. (5), where the inductance matrix elements are generally large because the $L_{i,n+i}$ (i=1,n) are negative, and the induced speed voltages in the right-hand side of Eq. (5) are reduced by half. For the best situation, assuming the superconducting coils to be far away from the null-flux equilibrium point ($G_{ij} >> G_{n+i,j}$), the current induced in the null-flux coil guideway is only about one-half of that in the loop-shaped coil guideway. From the view-point of the lumped circuit parameters, the resistance and the self-inductance in each null-flux coil are two times larger than that in a single loop coil. It is seen from Eq. (6) to Eq. (8) that the time-varying magnetic forces depend on the products of the currents in the null-flux coils and superconducting coils and the difference of the derivatives of the mutual inductances between the upper and lower loops. Thus, it can be concluded that the forces in the null-flux coil guideway, in general, are smaller than in the single loop-shaped coil suspension. However, it should be noted that the figure-eight null-flux coil suspension can produce both the null-flux lift and guidance forces, whereas a single set of loop-shaped guideway coils cannot generate both forces. Furthermore, the lift-to-drag ratio of the null-flux suspension can be several times higher than that of other EDS suspensions. Detailed performance of the null-flux suspension is discussed in the next section.

3. COMPUTER SIMULATION RESULTS AND DISCUSSION

To demonstrate the capability of the dynamic circuit model and to understand the performance of a maglev system using the null-flux suspension concept, a maglev system using side-wall null-flux suspension that has similar dimensions as those given in Tanaka's paper [6] is used as a numerical example. Figure 4 shows the cross-sectional view of the system on which the computer simulations were based. Table 1 gives its corresponding dimensions. A number of computations were conducted with various parameter ranges, such as the three dimensional magnetic forces as functions of air-gap, vertical displacement, lateral displacement, vehicle speed, and other parameters. Figure 5 to Fig. 14 illustrate the performance predictions for the null-flux suspension system under the various conditions. The dependence of magnetic forces on the dimensions of the figure-eight null-flux coils are also discussed. The simulation results show that the maglev system, using figure-eight null-flux suspension has many potential advantages over other systems, including a high vertical stiffness and a very high lift-to-drag ratio.

3.1 Force Characteristics of Null-flux Suspension

Figure 5 shows the dependence of the null-flux lift and guidance forces per SCM and the lift-to-drag ratio on vehicle velocity. It is observed from Fig. 5 that the null-flux levitation system can achieve very high lift-to-drag ratios, typically about 250 at 500 km/h with a vertical offset of 3 cm. However, the ratio drops sharply as the vertical offset increases. This implies that it is necessary for the null-flux suspension to operate at a small value of the vertical offset in order to show its major advantage over other systems and to achieve a high system efficiency. The lift force at this normal operation point is

about 15 kN/magnet, or 180 kN for a 12-magnet vehicle. This is sufficient to lift a vehicle of 17 to 18 tonnes.

Figure 5 also shows that the lift force approaches a maximum value of 42 kN/SCM at about 10- to 12-cm maximum vertical offset, or maximum vertical displacement. Beyond 12-cm offset the lift force decreases, meaning that the suspension system becomes unstable. However, the lateral guidance force of the system is much smaller than the lift force for vertical displacements of less than about 6 cm. This means that in the range where the lift-to-drag ratio is large, the guidance force is relatively small. Figure 6 illustrates force-speed characteristics for the null-flux suspension. As expected, it is similar to any other electrodynamic suspension systems. Both lift and guidance forces increase as the speed increases. The lift-to-drag and guidance-to-drag ratios are proportional to the vehicle speed, however, their slopes are quiet different. At a speed of 500 km/h, the former is 250 and the latter is only 50. High lift-to-drag ratio is a unique feature of null-flux suspension. It is important to note that the guidance-to-drag ratio of 50 for a null-flux suspension is similar to the lift-to-drag ratio in a loop-shaped coil suspension system.

Another important feature of figure-eight null-flux coil suspension is its large vertical stiffness. Figure 7 illustrates the null-flux lift and vertical stiffness per SCM as a function of vertical displacement with the equivalent air-gap as a parameter. It is seen from Fig. 7 that, for a vehicle having an air-gap of 20 cm and a speed of 500 km/h, the stiffness is about 5 kN/cm per SCM, or 60 kN/cm for a 12-SCM vehicle when its vertical displacement is around 2 to 3 cm. If a vehicle can carry 40 passengers, each weighing 80 kg, it will only be lowered by 5 mm from the empty to fully loaded state.

Computations were made on a pair of SCMs aboard the vehicle in which one SCM interacts with the right side-wall and the other interacts with the left side-wall. From this simulation, one is able to see the performance of the system under lateral disturbances. Figure 8 demonstrates the dependence on lateral displacement of the magnetic forces acting on the pair of SCMs. The total lift force (i.e., the sum of the lift forces on the two SCMs) has a minimum when the vehicle is centered. In addition, the lift force on each individual SCMs varies strongly with lateral displacement, whereas the total guidance force varies only weakly with displacement. In fact, the lift force per SCM almost doubles as the lateral displacement increases to 5 cm. The large imbalance in the lift forces on the left and right sides of the vehicle under large lateral displacements will lead to a roll motion of the vehicle. In addition, because of the increase in total lift with lateral displacement, the center of mass of the vehicle will also move upward with lateral displacement. The extent of the roll motion depends not only on the lateral shift but also on the vertical stiffness of the lift force (see Fig. 7). For example, a lateral shift of 2 cm increases the lift of one SCM from 14 to 20 kN, and reduces the lift on the other SCM from 14 to 12 kN, as shown in Fig. 8. From Fig. 7, it is seen that reducing the air-gap from 20 to 18 cm (i.e., a 2-cm lateral shift) would result in a decrease in vertical displacement of about 1.1 cm. An increase in air-gap from 20 to 22 cm would result in an increase in vertical displacement of about 0.5 cm. For a 3-m-wide vehicle, the angle of rotation would be about 0.31^{o}. Hence, provided that the vertical stiffness is very large, even if the lateral displacement is relatively large, the angle of rotation will remain relatively small (of the order of one or two degrees at most). Such roll motions may be regarded as unacceptable.

The lateral guidance acting on a pair of SCMs is relatively small, as shown in Fig. 8 and Fig. 9. As a consequence, the lateral stiffness is relatively small, as shown in Fig. 10 for a vertical offset of 3 cm. As the vertical offset increases to 7 cm, the lateral

stiffness increases substantially, as shown in Fig. 11. Unfortunately, such large vertical offsets result in substantially reduced lift-to-drag ratios (from about 260 at 3 cm to 100 at 7 cm, according to Fig. 7). Hence, if large lift-to-drag ratios are desired, and at the same time only small lateral displacements and associated rolling motions caused by perturbing lateral forces can be tolerated, alternative means of enhancing the lateral stiffness must be sought.

3.2 Enhancement of the Lateral Stiffness

The second generation of Canadian maglev design, as well as the Japanese MLU001 and MLU002 systems incorporated cross-connected propulsion windings to achieve a type of null-flux guidance. Such a scheme can be combined with the vertical mounted figure-eight null-flux suspension coils to achieve enhanced lateral guidance. Alternatively, as shown by Fujiwara and Fujimoto, it is also possible to cross-connect the figure-eight null-flux coils themselves to achieve null-flux operation for both the lift and guidance functions. In fact, they found that by this type of cross coupling, the lateral stiffness can be increased by a factor of 5 to 10. In addition to cross connections, changing the coil parameters may also result in improved null-flux coil performance, as indicated in the following discussion.

3.3 Effects of the Figure-Eight Coil Dimensions

It is important to determine the dimensions of figure-eight null-flux coils that can optimize system performance. Sensitivity studies were conducted on several key dimensions of the null-flux coils. The results are very interesting. Figure 12 illustrates the dependence of maximum lift force on the distance between the upper and the lower loops of the figure-eight coil. It is seen from Fig. 12 that the maximum lift force varies as the distance between two loops increases, and it approaches a peak of about 44 kN at a distance of about 20 cm. This means that the previous computation, based on a 12-cm distance between the loops that corresponds to a 42-kN maximum lift force, is not an optimum condition. Furthermore, since the vertical stiffness is closely related to the maximum lift force, one may control the vertical stiffness by varying the distance between two loops of the figure-eight null-flux coils.

Figure 13 shows the null-flux lift per SCM and the lift-to-drag ratio as a function of vehicle velocity with the length (longitudinal direction) of the figure-eight null-flux coil as a parameter. It is observed from Fig. 13 that the lift force increases only by about 10% as the length of the figure-eight coil increases from 45 to 65 cm. However, the lift-to-drag ratio increases by about 50%. It is obvious that, since the resistance of the null-flux coil is proportional to the length of the coil, magnetic drag in the system increases as the length of the coil increases. Thus, it seems that relatively short coils can have better lift-to-drag ratio. However, if the null-flux coil is too short, the coupling between the SCMs and the null-flux coils becomes poor, and the lift-to-drag ratio will also be reduced. In addition, the cost of a guideway is closely related to the dimensions of the figure-eight null-flux coil. A proper selection of the null-flux coil length can improve the suspension performance and reduce the guideway cost. Numerical studies show that the length of the coil plus the space between the two adjacent coils should be about one-third of the length of the SCMs.

3.4 Time Dependence Magnetic Forces

All of the magnetic forces in the null-flux suspension system fluctuate as the vehicle moves along the guideway. The amplitude of the fluctuation depends strongly upon the coil length and the spacing between coils. The pole-pitch of the null-flux coil is one of the major factors. Figure 14 shows the dependence of the null-flux lift on the longitudinal position of the SCM with the distance between two figure-eight coils as a parameter. It is seen from Fig. 14 that the figure-eight coil suspensions having 10 and 25-cm coil spacings suffer from large force fluctuations, and those having 15 and 20-cm coil spacings have small force fluctuations. There seems to be an optimum space at around 17 cm that minimizes the force fluctuations. However, the average forces always increase as the spacing decreases. It is interesting to note from Fig. 14 that the frequency of the force fluctuation is given by the vehicle speed divided by the length of the figure-eight coil plus the spacing between two neighbor coils. In Fig. 14, the length of the coil is 55 cm and vehicle velocity is 500 km/h for all four conditions. Thus, the frequencies of the force fluctuations are 214 Hz for 10-cm spacing, 198 Hz for 15-cm spacing, 185 Hz for 20-cm spacing, and 174 Hz for 25-cm spacing, respectively.

4. CONCLUDING REMARKS

The dynamic circuit model is a useful tool for studying a maglev system involving moving conducting coils. It can simulate the dynamic performance of the system and, in particular, be used to calculate the spatial and temporal variations in the magnetic forces.

The figure-eight-shaped null-flux side-wall suspension system has many advantages over other suspension systems. In particular, it has a simple configuration and can provide very high lift-to-drag ratios. The null-flux lift force depends strongly on both vertical and lateral displacement. The lateral guidance force of the side-wall suspension system is relatively weak and must be enhanced to provide stability against excessively large lateral displacements that could lead to role instability. Additional configurations are needed to increase the lateral guidance force in the system.

Further studies should be performed on the following areas: (1) optimum design of the null-flux side-wall suspension system, (2) interactions between components of the propulsion and suspension systems, and (3) vehicle dynamics under the influence of these magnetic forces.

ACKNOWLEDGMENT

Work supported by the U.S. Army Corps of Engineers, the Federal Railroad Administration, and Argonne National Laboratory through interagency agreements E8691R001 and DTFR53-91-X-00018, respectively, with the U.S. Department of Energy.

REFERENCES

[1] Danby, G.T., and Powell, J.R., Design Approaches and Parameters for Magnetically Levitated Transport Systems, Superconductivity and Its Applications. Elsevier Science Publishing Co., Inc., 1988. pp. 318-342.

[2] Hayes, W.F., and Tucker, H.G. , Design Concept and Comparative Performance of an Electrodynamic Maglev Transportation System for Toronto-Montreal

Corridor of Canada. IMechE 1984 c400/84. pp.137-148.
[3] Fujiwara, S., Characteristics of EDS Maglev Having Levitation Coils on the Side-wall of the Guideway. Quarterly Report, Railway Technical Research Institute, Japan, Vol. 29, No. 4, Nov, 1988. pp. 157-163.
[4] Fujiwara, S., and Fujimoto, T., Characteristics of the Combined Levitation and Guidance System Using Ground Coils on the Side-wall of the Guideway. International Conf. Maglev'89, July 1989. pp. 241-244.
[5] Fujimoto, T., and Fujiwara, S., Electrodynamic Characteristics of MLU002. Quarterly Report, Railway Technical Research Institute, Japan, Vol. 32, No. 2, June, 1991. pp. 50-58.
[6] Tanaka, H., Change in the Coil Distribution of Electrodynamic Suspension System. International Symposium on Magnetic Suspension Technology, NASA Langley Research Center, Hampton, Virginia, 23665-5225, USA, August 19-23, 1991.
[7]. Saitoh, T., Miyashita, K., and Kiwaki, H., Study for Harmonic Ripple of Electromagnetic Force in Superconducting Magnetically Levitated Vehicle with Non-Rectangular Ground Coils. International Conf. Maglev'89, July 1989. pp. 245-250.
[8] He, J.L., Rote, D.M., and Coffey, H.T. Computation of Magnetic Suspension of Maglev Systems Using Dynamic Circuit Theory. International Symposium on Magnetic Suspension Technology, NASA Langley Research Center, Hampton, Virginia, 23665-5225, USA, August 19-23, 1991.

Table 1 DATA USED FOR COMPUTER SIMULATION

Vehicle		
Total Weight	17	tonnes
Maximum Velocity	500	km/h
Height	3.7	m
Width	3	m
Number of SCMs	12	
Superconducting Magnet		
Length (x-direction)	1.7	m
Width (z-direction)	0.5	m
Gap between magnets	0.4	m
Current	700	kA-turn
Ground Null-Flux Coil		
Length	0.55	m
Width	0.31	m
Distance between upper and lower loops	0.12	m
Distance between null-flux coils	0.15	m
Number of turns	36	
Al conductor	1 cm^2	(cross-section)

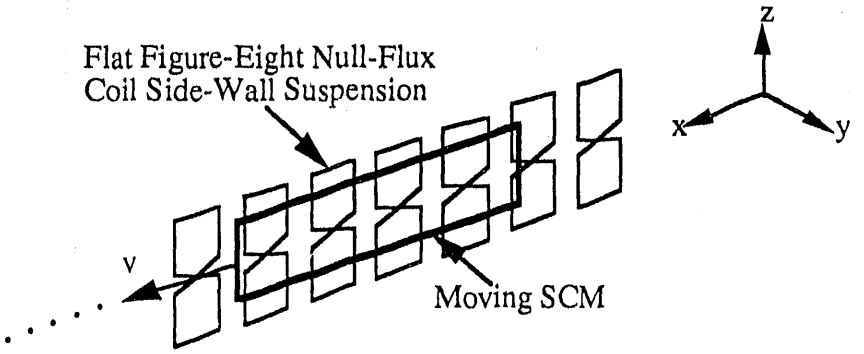

Fig. 1 A Superconducting Coil Moving along a Flat Figure-Eight-Shaped Null-Flux Coil Guideway (Side-Wall Suspension)

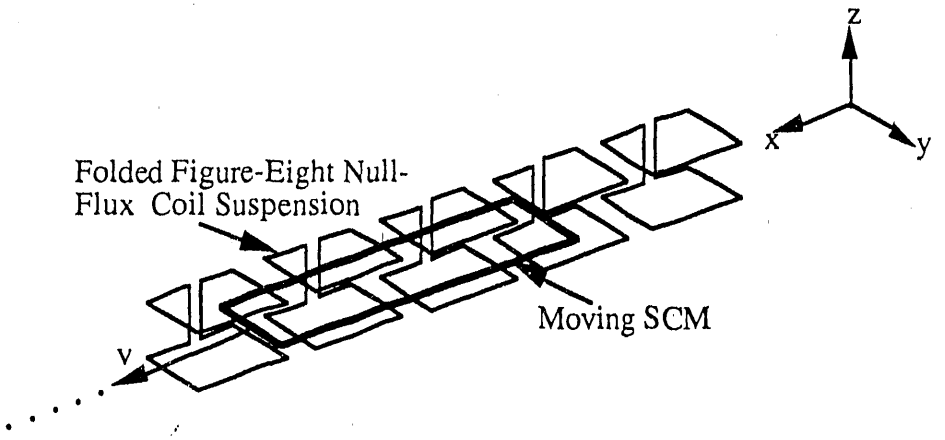

Fig. 2 A Superconducting Coil Moving above a Folded Figure-Eight-Shaped Null-Flux Coil Guideway

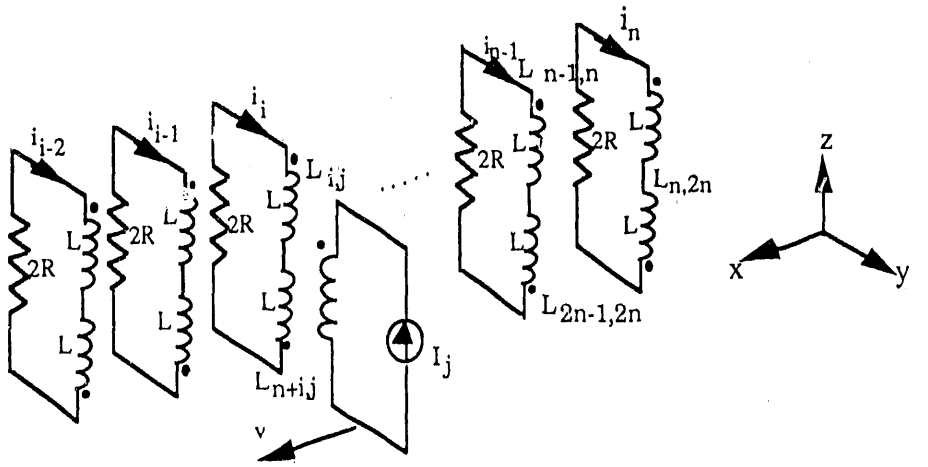

Fig. 3 Dynamic Circuit Representation of the Flat and Folded Figure-Eight-Shaped Null-Flux Coil Suspensions (only One SCM Shown)

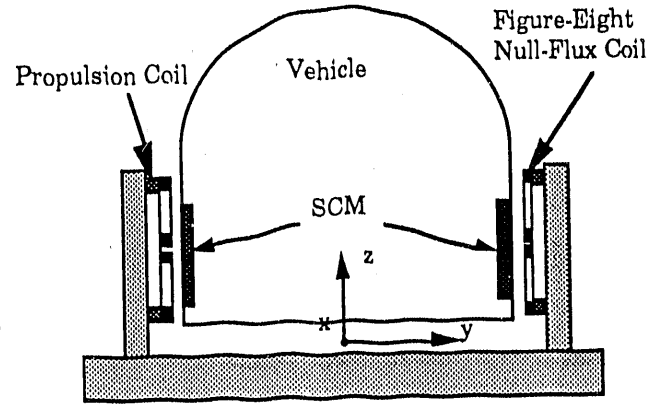

Fig. 4 Cross-Sectional View of a Side-Wall Null-Flux Levitation System

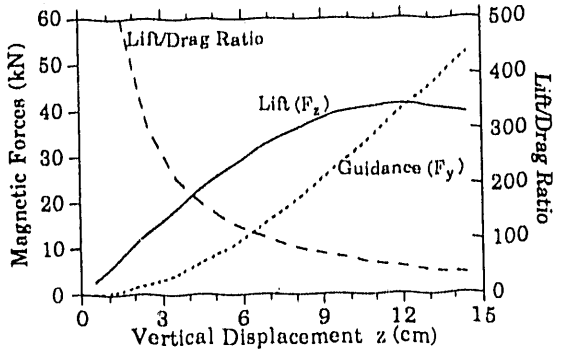

Fig. 5 Null-Flux Lift, Lateral Guidance, and Lift-to-Drag Ratio per SCM as a Function of Vertical Displacement. Air-Gap: 20 cm; Velocity: 500 km/h.

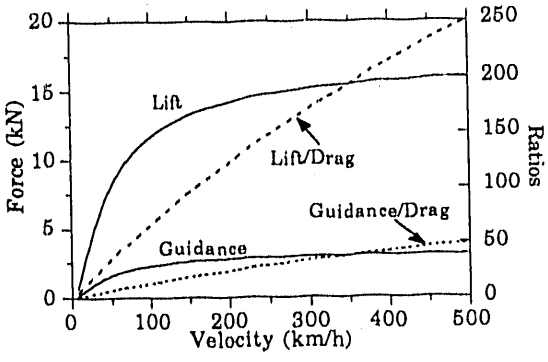

Fig. 6 Lift, Guidance, Lift-to-Drag Ratio, and Guidance-to-Drag Ratio as a Function of Vehicle Speed. Air-gap: 20 cm; Vertical-Offset: 3 cm.

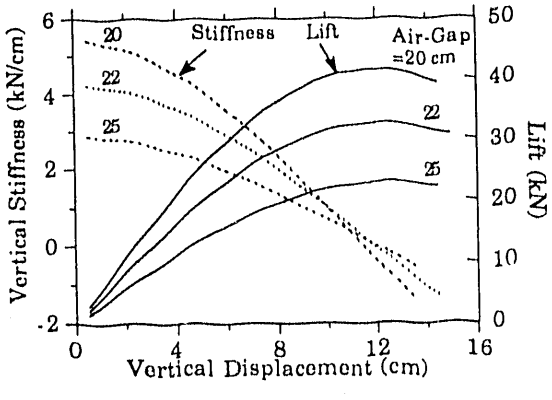

Fig. 7 Null-Flux Lift and Vertical Stiffness per SCM as a Function of Vertical Displacement. Velocity: 500 km/h; Parameter: Air-Gap .

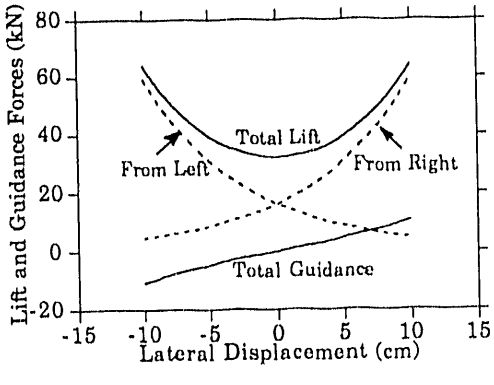

Fig. 8 Magnetic Forces Acting on SCM Pair as a Function of Lateral Displacement. Velocity: 500 km/h; Air-gap: 20 cm; Vertical Offset: 3 cm.

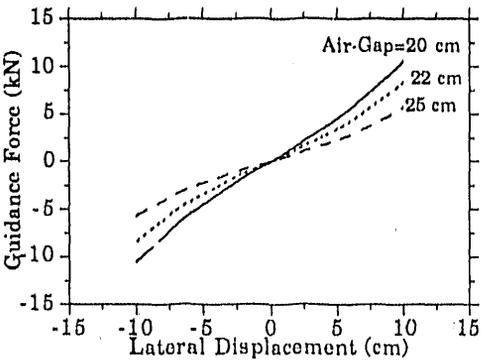

Fig. 9 Guidance Force on SCM Pair as a Function of Lateral Displacement with Air-Gap as a Parameter

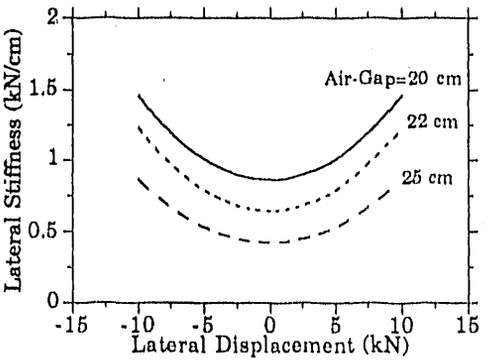

Fig. 10 Lateral Stiffness as a Function of Lateral Displacement with Air-Gap as a Parameter

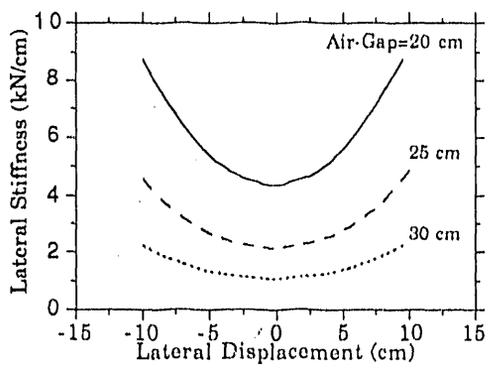

Fig. 11 Lateral Stiffness as a Function of Lateral Displacement with Air-Gap as a Parameter. Velocity: 500 km/h; Vertical Offset: 7 cm.

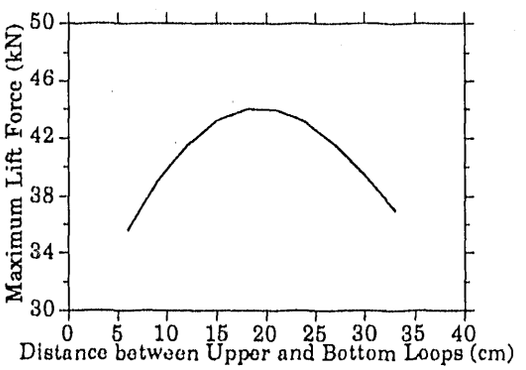

Fig. 12 Maximum Lift Force as a Function of Loops. the Distance between Upper and Lower Loops Air-gap: 20 cm; Velocity: 500 km/h.

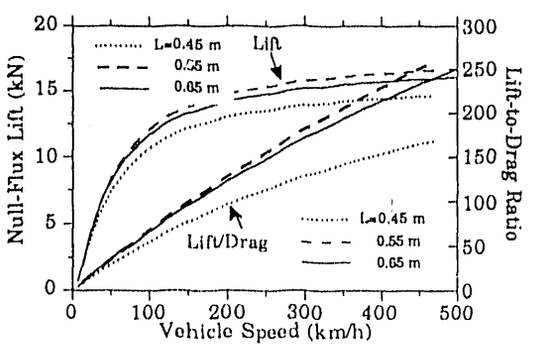

Fig. 13 Dependence on Velocity of Null-Flux Lift per SCM and Lift-to-Drag Ratio with the Length of Figure-Eight Coil (L) as a Parameter. Vertical-Offset: 3 cm; Air-Gap: 20 cm

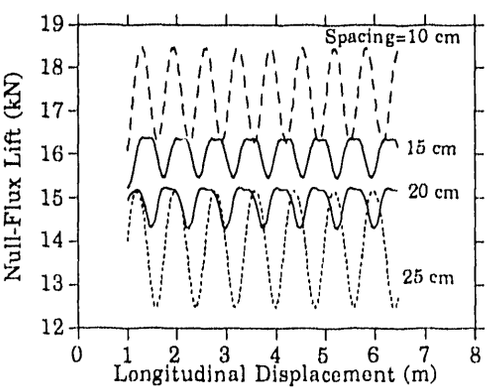

Fig. 14 Null-Flux Lift Force as a Function of Longitudinal Displacement with the Spacing between the Figure-Eight Coils as a Parameter.